Australian Journal of Earth Sciences
An International Geoscience Journal of the Geological Society of Australia
Publication details, including instructions for authors and subscription information:
http://www.informaworld.com/smpp/title~content=t716100753

Gold deposits of the Bardoc Tectonic Zone: a distinct style of orogenic gold in the Archaean Eastern Goldfields Province, Yilgarn Craton, Western Australia

Online Publication Date: 01 August 2007
To cite this Article: Morey, A. A., Weinberg, R. F., Bierlein, F. P. and Davidson, G. J. , (2007) 'Gold deposits of the Bardoc Tectonic Zone: a distinct style of orogenic gold in the Archaean Eastern Goldfields Province, Yilgarn Craton, Western Australia', Australian Journal of Earth Sciences, 54:6, 783 - 800
To link to this article: DOI: 10.1080/08120090701392671
URL: http://dx.doi.org/10.1080/08120090701392671

Australian Journal of Earth Sciences (2007) **54**, (783–800)

Gold deposits of the Bardoc Tectonic Zone: a distinct style of orogenic gold in the Archaean Eastern Goldfields Province, Yilgarn Craton, Western Australia

A. A. MOREY[1], R. F. WEINBERG[1], F. P. BIERLEIN[2]* AND G. J. DAVIDSON[3]

[1]*Predictive mineral discovery*Cooperative Research Centre, Australian Crustal Research Centre, School of Geosciences, Monash University, Vic 3800, Australia.*

[2]*Centre for Exploration Targeting and Tectonics Special Research Centre, School of Earth and Geographical Sciences, University of Western Australia, 35 Stirling Highway, Crawley, WA 6009, Australia.*

[3]*ARC Centre of Excellence in Ore Deposits, School of Earth Sciences, University of Tasmania, Private Bag 79, Hobart, Tas. 7001, Australia.*

The Bardoc Tectonic Zone is an ~80 km-long and up to 12 km wide, intensely sheared corridor of Late Archaean supracrustal rocks that is bounded by pre- to syn-tectonic granites in the Eastern Goldfields Province, Yilgarn Craton. This zone has produced over 100 t of gold from a range of deposits, the largest being Paddington (~40 t Au). This shear system is connected along strike to the Boulder–Lefroy Shear Zone, which hosts considerably larger deposits including the giant Golden Mile Camp (>1500 t produced Au). In contrast to the diverse characteristics of gold deposits associated with the Boulder–Lefroy Shear Zone, mineralogical and geochemical data from five representative localities in the Bardoc Tectonic Zone have relatively uniform features. These are: (i) quartz–carbonate veins in competent mafic units with wall-rock alteration characterised by carbonate + quartz + muscovite + chlorite ± biotite + sulf-arsenide + sulfide + oxide + gold assemblages; (ii) arsenopyrite as the dominant sulfur-bearing mineral; (iii) a unique three-stage paragenetic history, commencing with pyrrhotite, and progressing to arsenopyrite and then to pyrite-dominated alteration; (iv) a lack of minerals indicative of oxidising conditions, such as hematite and sulfates; (v) δ^{34} sulfur compositions of pre- to syn-gold iron sulfides ranging from 1 to 9‰; and (vi) a lack of tellurides. These features characterise a coherent group of moderately sized orogenic-gold deposits, and when compared with the larger gold deposits of the Boulder–Lefroy Shear Zone, potentially highlight the petrological and geochemical differences between high-tonnage and smaller deposits in the Eastern Goldfields Province.

KEY WORDS: Archaean, Bardoc Tectonic Zone, hydrothermal alteration, orogenic gold, sulfur isotopes, Yilgarn Craton.

INTRODUCTION

The Late Archaean Eastern Goldfields Province of the Yilgarn Craton hosts at least one giant (≥500 t Au) and over 10 world-class (≥100 t Au) orogenic-gold deposits (Hagemann & Cassidy 2001). These deposits are primarily located along major shear zones and their subordinate fault systems (Groves *et al.* 1984; Eisenlohr *et al.* 1989). Due to the broad range of geological conditions over which orogenic-gold deposits form (Groves 1993; Groves *et al.* 1998; Witt & Vanderhor 1998; Hagemann & Cassidy 2001), these systems display a wide range of characteristics such as variations in vein style, metamorphic grade, host lithologies, hydrothermal alteration, interpreted fluid/rock ratios and redox conditions. This diversity requires that exploration models for orogenic-gold deposits be reassessed and modified to suit specific target areas, even at the camp to district scale. This is demonstrated by studying orogenic-gold mineralisation in the Bardoc Tectonic Zone, which hosts relatively small gold deposits (<40 t Au) with uniform features over its ~80 km length. This uniformity is very distinct from the larger (>100 t Au) deposit characteristics in the connecting Boulder–Lefroy Shear Zone. In this paper, we first describe the nature of sub-world-class mineralisation, hydrothermal alteration and sulfur isotope data of five localities in the Bardoc Tectonic Zone. These include the Paddington, Talbot South, New Boddington and Yunndaga gold deposits, and the Nerrin Nerrin gold prospect (Figure 1). As the Paddington gold deposit is located near the intersection of the Bardoc Tectonic Zone and Boulder–Lefroy Shear Zone, this study also assesses the regional setting of this significant structural boundary. By comparing

*Corresponding author: bierlein@cyllene.uwa.edu.au

ISSN 0812-0099 print/ISSN 1440-0952 online © 2007 Geological Society of Australia
DOI: 10.1080/08120090701392671

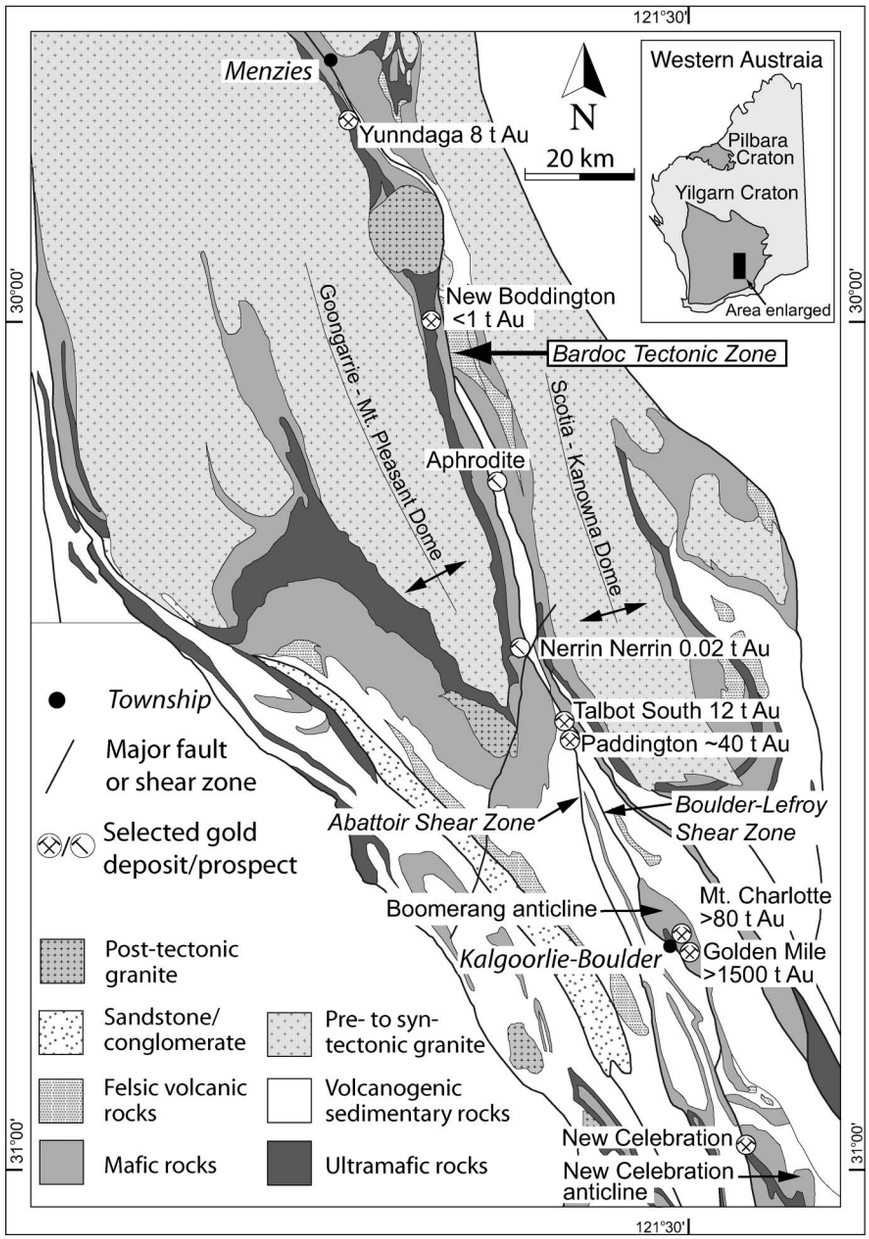

Figure 1 Geological map of part of the southern Eastern Goldfields Province, Yilgarn Craton, Western Australia showing the localities related to this study and selected gold deposits and camps (modified from Witt & Swager 1989; Swager & Griffin 1990a).

mineralisation styles of the Bardoc Tectonic Zone with the much larger deposits of the Boulder–Lefroy Shear Zone and other world-class gold deposits in the Eastern Goldfields Province, it is possible to further define the major characteristics of large and small, shear zone-hosted orogenic-gold deposits.

BARDOC TECTONIC ZONE

The Bardoc Tectonic Zone is an ~80 km-long, north-northwest-trending regional shear system that separates two distinctive tectono-stratigraphic domains in the multiply deformed Eastern Goldfields Province (Figure 1) (Swager *et al.* 1995; Goleby *et al.* 2002). The Bardoc Tectonic Zone is unique at least in the Eastern Goldfields Province, in that it is a system in which intense strain is distributed within a <12 km wide corridor of supracrustal rocks between competent pre- to syn-deformation granites (*sensu stricto*), the Scotia–Kanowna Dome to the east and the Goongarrie–Mt Pleasant Dome to the west. Whereas many orogenic-gold deposits in the Eastern Goldfields Province are sited on second- or third-order structures that splay off first-order shear systems (Eisenlohr *et al.* 1989), the Bardoc Tectonic Zone-hosted gold deposits are situated within the wide zone of shearing itself (Witt 1993).

In the Bardoc Tectonic Zone, lithological contacts and internal foliations trend north-northwest and generally dip steeply to the west. Major lithologies include mafic and ultramafic extrusive rocks, both with various interflow shale units, intruded by dolerites and gabbros, and less commonly by felsic intrusive units (Witt 1994). These rock units are unconformably overlain by volcanogenic sedimentary rocks known regionally as the Black Flag Group (Hunter 1993). Even though there is a

large degree of structural disruption and attenuation, a number of lithologies can be traced along the length of the shear zone from Paddington to Menzies (Figure 1) (Witt 1994). Previous work (Witt 1993; Beeson *et al.* 1996), shows that all lithologies can host gold mineralisation, although recent and historical gold production is chiefly from mafic extrusive and intrusive units. Metamorphism is mostly of greenschist facies, except close to the bounding granites (Mikucki & Roberts 2004), and in the Menzies area to the north (Figure 1) where the metamorphic grade increases to lower amphibolite facies (Witt 1992, 1993; Beeson *et al.* 1996). Strain is variably localised, with less competent ultramafic and sedimentary units being more strongly deformed than the more competent granitic and mafic units. In the southern Eastern Goldfields Province, which includes the Bardoc Tectonic Zone, four major shortening events have been identified, starting with thin-skinned thrust stacking indicating approximately north–south shortening (D_1), followed by a major inclined to upright folding and reverse faulting episode on north-northwest-trending planes (D_2) that was also associated with localised orogen-parallel extension (Davis & Maidens 2003). Continued shortening formed oblique-sinistral motion on north-northwest-trending shear zones (D_3), and later by dominantly northeast-trending, brittle–ductile oblique-slip faulting (D_4). The major (D_2–D_4) deformation events are consistent with regional east-northeast–west-southwest shortening (Swager & Griffin 1990b; Swager 1997; Weinberg *et al.* 2003).

Based on their geologic setting, styles and hydrothermal alteration assemblages, the gold deposits studied in the Bardoc Tectonic Zone are considered to be orogenic (Witt 1992, 1993). Gold is generally associated with epigenetic quartz–carbonate veins and/or shear zones, which formed during the major east-northeast–west-southwest shortening event that produced upright folds and reverse shear zones. Northward from Paddington to Menzies, veins are hosted in structures that generally become more ductile in nature, which also corresponds to a progressive change from greenschist facies metamorphic assemblages in the south to lower amphibolite facies assemblages in the northern part of the shear system (Witt 1993; Beeson *et al.* 1996; Mikucki & Roberts 2004). Wall-rock hydrothermal alteration minerals associated with mineralised veins typically consist of quartz, carbonate, chlorite, sericite, biotite, arsenopyrite, pyrite and base-metal sulfides, with a greater abundance of biotite alteration in the higher grade deposits towards the northern sections of the Bardoc Tectonic Zone (Beeson *et al.* 1996).

FIELD SITES AND ANALYTICAL TECHNIQUES

Thirty thin-sections were prepared from the Paddington (7), Talbot South (3), New Boddington (7) and Yunndaga (9) localities (Figure 1; Table 1). In the absence of surface exposure at Nerrin Nerrin, four thin-sections were obtained from drillcore from this prospect. The mineralogy, paragenesis and textures of mineral phases were analysed using optical, scanning electron microscopy (Jeol© JSM 6300 scanning electron microscope, SEM, at

Table 1 Major characteristics of each deposit/study locality.

Deposits from south to north	Gold mined (t Au)	Host lithology	Metamorphic facies of host lithology	Vein structure	Alteration assemblage[a] (in decreasing abundance)
Paddington laminated vein	~40	Dolerite and basalt	Greenschist	Shear vein	Carb, Qtz, Ms, Bt, Apy, other sulfides, Fe-oxides
Paddington ladder vein		Dolerite and basalt	Greenschist	Planar vein	Carb, Qtz, Ms, Apy, other sulfides, Fe-oxides
Talbot South	12	Gabbro	Greenschist	Brecciated and planar veins	Qtz, Carb, Ms, Chl, ± Bt, Apy, other sulfides, Fe-oxides
Nerrin Nerrin	0.02	Dolerite	Greenschist	Planar veinlets	Qtz, Carb, Ms, Chl, Apy, other sulfides, Fe-oxides
New Boddington	<1	Basalt	Greenschist	Stockwork & planar veins	Carb, Qtz, Chl, Bt, Ms, Apy, other sulfides, Fe-oxides
Yunndaga	8	Contact between sedimentary rock and dolerite	Lower amphibolite	Shear laminated vein	Qtz, Carb, Bt, Ms, Apy, other sulfides, Fe-oxides

[a]Apy, arsenopyrite; Bt, biotite; Carb, carbonate; Chl, chlorite; Ms, muscovite; Qtz, quartz.

the University of Ballarat) and energy dispersive X-ray spectrometry (EDS). Analytical conditions for the SEM were 15 kV and 1.5 nA. Backscattered images on the SEM were acquired using an Oxford Instruments four-element quadrant detector.

Sulfur isotope analyses were carried out at the Central Science Laboratory, University of Tasmania, Hobart. *In situ* laser ablation (Huston *et al.* 1995) and conventional digestion techniques (Robinson & Kasakabe 1975) were applied on selected sulfide-bearing samples. Stable sulfur isotope ratios (δ^{34}S) are reported relative to the Canyon Diablo Troilite (CDT) in parts per mil (‰). Error margins are quoted in Tables 2 and 3, and precision values for *in situ* and conventional analyses are typically 0.05‰ and 0.1‰, respectively (Huston *et al.* 1995).

In situ major- and trace-element analyses of representative sulfide phases were carried out with a laser-ablation inductively coupled plasma-mass spectrometer (LA-ICP-MS), at the Centre of Ore Deposit Research, University of Tasmania, Hobart. Twenty-six major and trace elements were analysed (Ti, Cr, Mn, Fe, Co, Ni, Cu, Zn, As, Se, Zr, Mo, Ag, Cd, Sn, Sb, Te, Ba, W, Au, Tl, Pb, Bi, La, Th and U) using a New Wave OP213 laser probe and HP4500 quadrupole ICP-MS. As this analysis was used to detect the presence of gold in sulfides/sulf-arsenides, only gold and silver data are presented here (Table 4). Calibration techniques follow Danyushevsky *et al.* (2003) and Norman *et al.* (2003), where data were quantified with the use of a primary standard (STDGL2b-2). Ablation spot sizes varied between 8 and 30 μm at a frequency of

Table 2 Sulfur isotope data from mineralised rock samples.

Location	Analysis type[a]	Sample details	δ^{34}S (‰)
Paddington	ISLA	Stage 3 Py	2.9
Paddington	ISLA	Stage 3 Py	4.2
Paddington	ISLA	Stage 3 Py	5.6
Paddington	ISLA	Inner core of stage 3 Py	2.7
Paddington	ISLA	Outer rim of stage 3 Py	6.9
Paddington	ISLA	Stage 3 Py	5.6
Paddington	ISLA	Stage 3 Py	5.9
Paddington	ISLA	Inner core of Stage 3 Py	3.4
Paddington	ISLA	Stage 2 Apy	2.7
Paddington	ISLA	Inner core of Stage 2 Apy	7.5
Paddington	ISLA	Outer rim of Stage 2 Apy	5.8
Paddington	ISLA	Inner core of Stage 2 Apy	6.7
Paddington	ISLA	Outer rim of Stage 2 Apy	6.3
Paddington	ISLA	Inner core of Stage 2 Apy	8.2
Paddington	ISLA	Outer rim of Stage 2 Apy	8.1
Talbot South	Conventional	Mineralised gabbro, whole-rock sample	2.25
Talbot South	ISLA	Stage 2 Apy	5.2
Talbot South	ISLA	Stage 2 Apy	5.8
Talbot South	ISLA	Stage 2 Apy	7.0
Talbot South	ISLA	Stage 3 Py	1.9
Talbot South	ISLA	Stage 3 Py	2.9
Talbot South	ISLA	Stage 3 Py	2.9
Nerrin Nerrin	Conventional	Stage 2 Apy	1.58
Nerrin Nerrin	ISLA	Stage 3 Py—potential contamination by Sp	0.66
Nerrin Nerrin	ISLA	Stage 3 Py	2.8
Nerrin Nerrin	ISLA	Stage 3 Py	4.8
Nerrin Nerrin	ISLA	Stage 3 Py	6.2
Nerrin Nerrin	ISLA	Stage 2 Apy	5.7
Nerrin Nerrin	ISLA	Stage 2 Apy	7.9
New Boddington	ISLA	Stage 2 Apy	4.3
New Boddington	ISLA	Stage 2 Apy	4.3
New Boddington	ISLA	Stage 2 Apy	4.3
New Boddington	ISLA	Stage 2 Apy	6.0
New Boddington	ISLA	Stage 3 Po	3.5
Yunndaga	ISLA	Stage 3 Apy	0.14
Yunndaga	ISLA	Stage 3 Apy	0.96
Yunndaga	ISLA	Stage 2 Apy	4.0
Yunndaga	ISLA	Stage 2 Apy	5.8
Yunndaga	ISLA	Stage 2 Apy	6.3
Yunndaga	ISLA	Stage 2 Apy	5.3
Yunndaga	ISLA	Stage 2 Apy	5.7
Yunndaga	ISLA	Stage 3 Po	0.1

Apy, Arsenopyrite; Po, pyrrhotite; Py, Pyrite; Sp, sphalerite; ISLA, *In situ* laser ablation.
[a]Errors for conventional and ISLA analyses are $\pm$0.15 and $\pm$0.4, respectively.

Table 3 Sulfur isotope data from unmineralised rock samples.

Location	Analysis type[a]	Sample details	δ^{34}S (‰) type
Paddington	Conventional	Py separate from sulfidic shale	2.0
Paddington	ISLA	Py within sulfidic shale	3.2
Paddington	ISLA	Py within sulfidic shale	4.4
Paddington	ISLA	Py within sulfidic shale	4.6
Talbot South	ISLA	Py within sulfidic shale	2.8
Talbot South	ISLA	Py within sulfidic shale	3.5
Talbot South	ISLA	Py within sulfidic shale	4.0
Between Paddington & Talbot South	ISLA	Py associated with carbonate-dominated vein	2.7
Between Paddington & Talbot South	ISLA	Py within sulfidic shale	8.0
Between Paddington & Talbot South	ISLA	Py within sulfidic shale	3.9
Between Paddington & Talbot South	ISLA	Py within sulfidic shale	3.6
Between Paddington & Talbot South	ISLA	Py within sulfidic shale	3.4
South Duke	ISLA	Py within sulfidic shale	3.3
South Duke	ISLA	Py within sulfidic shale	4.1
South Duke	ISLA	Py within sulfidic shale	6.8
Yunndaga	Conventional	Py separate from sulfidic shale	2.2
Yunndaga	ISLA	Rim of Py grain within sulfidic shale	1.4
Yunndaga	ISLA	Py within sulfidic shale	2.4

Py, pyrite; ISLA, *in situ* laser ablation.
[a]Errors for conventional and ISLA analyses are ± 0.15 and ± 0.4, respectively.

Table 4 Invisible gold and silver concentrations (ppm) of Stage 2 arsenopyrite from quantitative LA-ICP-MS analyses.

Sample	Location	Au (ppm)	Ag (ppm)	Detection limit (ppm)	Precision (%)
Laminated vein S051910A-17	Paddington 341446E 6625231S	23	1.42	1	± 8
Ladder vein PD231609–18	Paddington 340945E 6626555S	11	<1	1	± 6
Talbot South BWRCD247B-27	Talbot South 339147E 6630276S	9.8	<1	1	± 9
Nerrin Nerrin NNDD001–11	Nerrin Nerrin 335680E 6639490S	8.2	<1	1	± 5
New Boddington GG011906B-9	New Boddington 323142E 6675085S	28	<1	1	± 5
Yunndaga YD10800–6	Yunndaga 311327E 6707386S	1.6	<1	1	± 14

5–10 Hz. Each analysis consisted of a 30 s background run and a 60 s analysis time. Analytical detection limits and precision data are provided in Table 4.

HYDROTHERMAL ALTERATION AND MINERAL PARAGENESIS RELATED TO GOLD MINERALISATION

All rock samples are from hydrothermal alteration selvages directly adjacent to quartz–carbonate veins hosted in mafic rocks. Table 1 outlines the characteristics of each mineralised locality and sketch maps of each study area with coordinates are shown in Figure 2. Other rock units can host gold mineralisation (Witt 1993), although production from gold deposits in the Bardoc Tectonic Zone is dominated by mafic-hosted vein and shear zone systems. Therefore, mafic-hosted units provide representative examples of gold mineralisation in the Bardoc Tectonic Zone. The overprinting relationships of different hydrothermal silicate minerals are ambiguous, and therefore the hydrothermal alteration history is derived from the overprinting relationships of the sulfide and oxide minerals. Abbreviations for mineral phases used in figures and tables are from Kretz (1983).

Paddington deposit

The Paddington gold deposit comprises two linked, elongate openpits that are aligned with the regional north-northwest trend of the Bardoc Tectonic Zone (Hancock *et al.* 1990; Alardyce & Vanderhor 1998) (Figure 2a). Between 1998 and 2000, 18 Mt of ore was mined, averaging 2.28 g/t Au, producing 37 t of gold

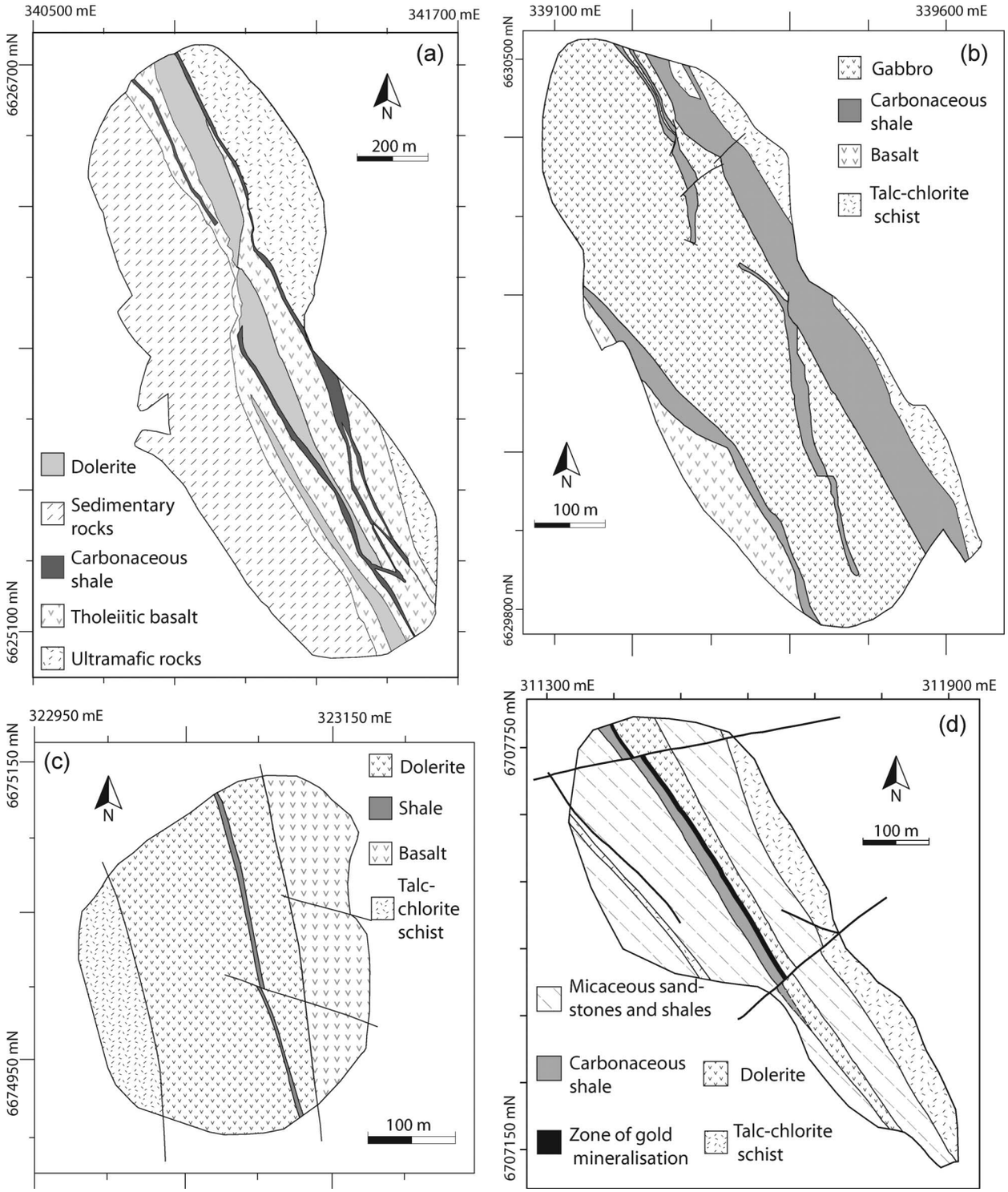

Figure 2 Lithology maps of the openpits covered in this study. Lithological units trend north-northwest and dip steeply to the west. The subsurface Nerrin Nerrin prospect is not shown. Geology is based on unpublished maps from Barrick Gold. See Figure 1 for locations of each deposit. (a) Paddington gold deposit. (b) Talbot South gold deposit. (c) New Boddington gold deposit. (d) Yunndaga gold deposit.

(Sheehan & Halley 2002). Rock units exposed in the openpits trend north-northwest and dip steeply west and east. The mineralisation is hosted by a dolerite unit in the northern pit, and by basalt in the southern pit. Both mineralised units are flanked on the west by volcaniclastic sedimentary rocks and on the east by talc–chlorite ultramafic schist. Interflow sulfidic and carbonaceous shales also occur in and at the boundaries of the basalt unit (Hancock *et al.* 1990).

There are two styles of mineralised structures at Paddington: (i) a single, continuous, quartz–carbonate laminated vein; and (ii) arrays of subhorizontal quartz–carbonate ladder veins (Alardyce & Vanderhor 1998; Sheehan & Halley 2002). The north-northwest-trending, steeply east-dipping laminated vein is up to 3 m thick and is characterised at its margins by alternating layers of quartz–carbonate and altered/mineralised wall-rock selvages, and is parallel to, and hosted within, a north-northwest-trending, steeply dipping, reverse-sense shear zone (Figure 3a). The ladder veins (Figure 3b) are defined by an array of gently dipping, thin veins ($\sim$2–5 cm wide) and, based on their planar nature and orientation at a high angle to the steeply dipping, north-northwest-trending pervasive foliation and associated stretching lineation, are interpreted as tension veins. Both vein styles are strikingly similar to mineralised structures at the greenstone-hosted Sigma Mine, Canada (Robert & Brown 1986). In both vein types, visible gold is dominantly located within the hydrothermal wall-rock alteration halo, which extends up to tens of centimetres away from the vein margins (Table 1; Figure 4). These assemblages are dominated by carbonate, quartz, muscovite, biotite (laminated vein), sulfides, oxide minerals, and visible gold (Table 1). EDS analyses show that the carbonate grains are dominated by calcite that generally contains up to 5 atomic % Fe (ferroan calcite). Muscovite has replaced biotite in the wall-rock selvages of the laminated vein, and alteration assemblages are more strongly deformed than those associated with the ladder veins (Figure 3c, d).

Arsenopyrite is the most abundant sulfur-bearing phase in the alteration zone of both vein styles. It occurs as euhedral grains up to 7 mm in length (Figure 3a) and has commonly undergone brittle fracturing (Figure 3c–f). The hydrothermal sulfur-bearing and oxide phases define three overprinting alteration stages. Stage 1 is characterised by abundant pyrrhotite inclusions in the cores of Stage 2 arsenopyrite grains (Figure 4) (Hancock *et al.* 1990). Even though isolated, these individual pyrrhotite inclusions within any particular arsenopyrite grain have identical extension angles in cross-polarised light, confirming that they are remnants of a single grain that pre-dated the formation of Stage 2 arsenopyrite. Stage 3 is the most complex hydrothermal stage, and is characterised by pyrite, chalcopyrite, galena (only documented in the laminated vein), rutile and visible gold (with silver up to 20 atomic %). Visible gold occurs in microfractures and along the grain boundaries of Stage 2 arsenopyrite grains (Figure 3e, f). In the laminated vein, pyrite also occurs in fine veinlets that cut across the vein laminations at a high angle. Scheelite (as reported by Booth 1989 and Hancock *et al.* 1990) was also documented as fine (=1 mm) grains within the hydrothermal alteration assemblage, but in contrast to the findings of Hancock *et al.* (1990), no marcasite was recorded in pyrite grains.

Talbot South deposit

Talbot South is located in the Broad Arrow Camp, 5 km north-northwest of Paddington (Figure 1). It produced 1.2 t of gold from 1903 to 1911 (Witt 1992). From the mid 1990s to 2000, openpit mining produced $\sim$12 t of gold (Manly 2003). The mineralised structures are located in a steep west-dipping, north-northwest-trending gabbro unit that is bounded on both sides by more intensely deformed sandstone and shale units (Figure 2b). In the openpit, the gabbro is up to 100 m in thickness and is only pervasively foliated at the contacts with the sedimentary rocks. The ore is associated with a strike-parallel, hydrothermal breccia zone, up to 8 m thick and dipping steeply to the east, characterised by a zone of intensified silicification and carbonation within the gabbro unit that extends for the length of the openpit (Figure 4) (Revell 2000).

Hydrothermal alteration minerals associated with the breccia zone include quartz, carbonate, muscovite, chlorite after biotite, sulfides and oxide phases (Figure 5a; Table 1). Quartz, carbonate and muscovite overprint primary plagioclase grains, and biotite is overprinted by chlorite, which also occurs in fractures in arsenopyrite (Figure 5b). In order of decreasing abundance, arsenopyrite, pyrite, chalcopyrite, ilmenite, pyrrhotite and visible gold also occur in the altered wall-rock. Overprinting relationships of the sulfur-bearing and oxide phases define a three-stage alteration history, analogous to those determined at Paddington (Figure 4). Stage 1 is defined by remnant pyrrhotite preserved as $<$0.5 mm rounded inclusions in Stage 2 arsenopyrite, which commonly has pitted cores hosting Stage 1 pyrrhotite and inclusion-free rims (Figure 5c inset). Like Paddington, Stage 3 is characterised by the fracturing and overprinting of arsenopyrite grains by coliform pyrite, chalcopyrite, visible gold and ilmenite (Figure 5c, d). The rare embayed nature of Stage 2 arsenopyrite grains (Figure 5c, d) suggests that minor hydrothermal corrosion occurred prior to or during the formation of Stage 3 phases.

Nerrin Nerrin gold prospect

Nerrin Nerrin is an exploration prospect in the Bardoc Tectonic Zone, 30 km north-northwest of Paddington (Figure 1). Locally, Witt (1992) reported historical production of 15.1 kg of gold from 1879 to 1919. Ultramafic, dolerite and carbonaceous sedimentary rock units have been intersected by diamond drilling (Manly 2003). The dolerite unit has been interpreted to be the northerly extension of the same mafic unit that hosts the Paddington and Talbot South gold deposits (Manly 2003). A 2 m core section in the dolerite unit at Nerrin Nerrin assayed an average of 1.32 g/t of gold, and used here to characterise the hydrothermal alteration history of this prospect.

Thin-section analyses reveal that the gold-bearing assemblage occurs in wall-rock adjacent to $<$5 cm wide quartz–carbonate veinlets (Figure 6a), in a $<$10 cm

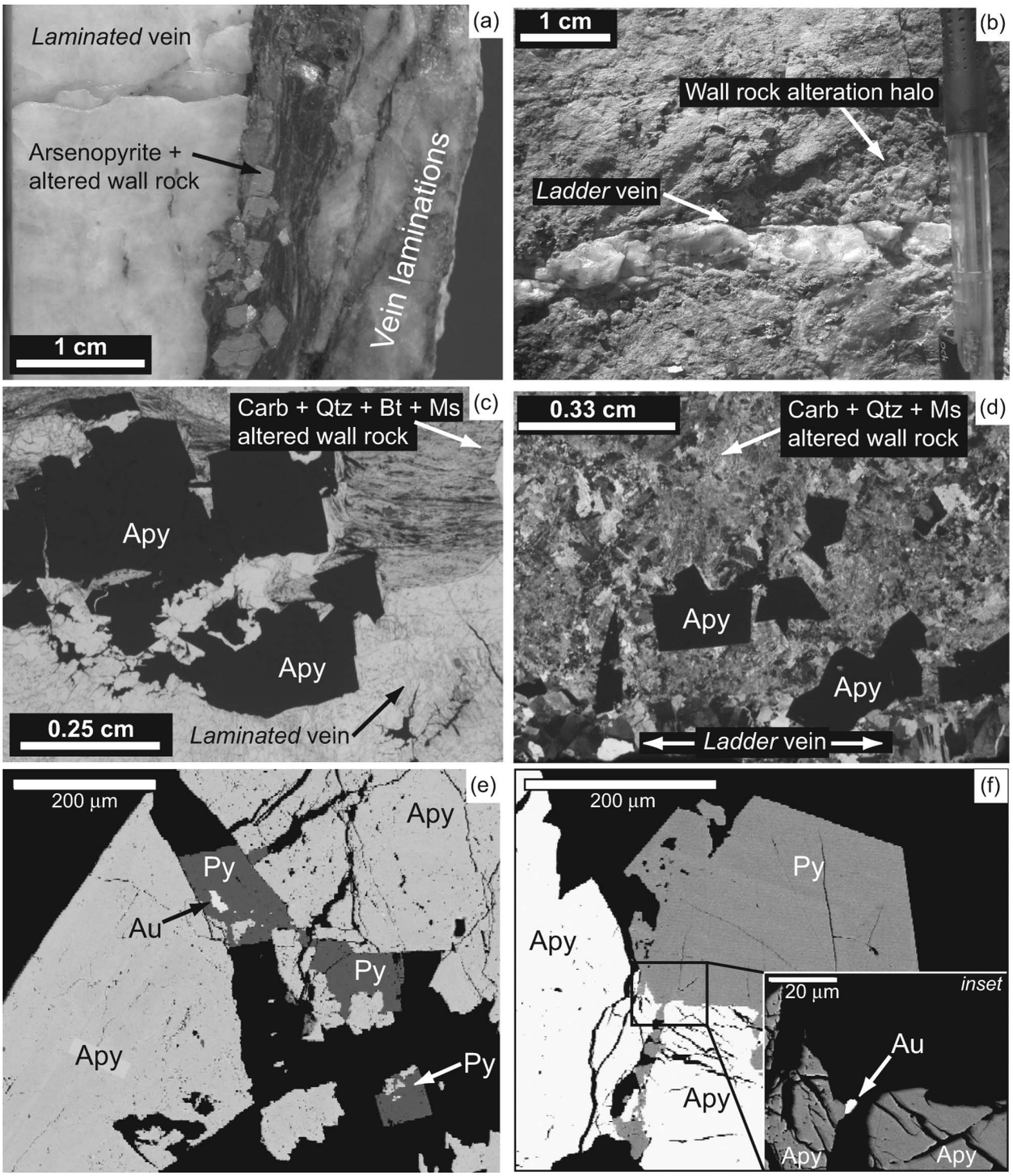

Figure 3 Photographs from the Paddington gold deposit. (a) Laminated vein showing characteristic alternating laminations of quartz–carbonate veins and hydrothermally altered and mineralised wall-rock (sample PD13a). (b) Ladder vein from Paddington. Vein thickness is 1–2 cm and sulfides (dominantly arsenopyrite) are located in a <10 cm-wide wall-rock alteration halo (GR 341263E, 6625687N). (c) Microstructure in cross-polarised light of the laminated vein margin and related hydrothermal silicate, carbonate and sulfide alteration assemblage. Note the fractured nature of the arsenopyrite grains (sample PD13b). (d) Cross-polarised photomicrograph of the hydrothermal assemblage associated with the ladder vein. Note the intense carbonate, silica, muscovite and sulfide wall-rock alteration proximal to the ladder vein (sample PD131). (e) Backscatter electron SEM image of Stage 3 pyrite and visible gold in a Stage 2 arsenopyrite fracture (sample PD235). (f) Backscatter electron SEM images of a Stage 2 arsenopyrite fracture infilled with pyrite. Inset: close-up of highlighted area with contrast adjusted to reveal Stage 3 visible gold in the arsenopyrite fracture (sample PD236). Apy, arsenopyrite; Au, visible gold; Bt, biotite; Carb, carbonate; Ms, muscovite; Py, pyrite; Qtz, quartz. All samples reposited at School of Geosciences, Monash University.

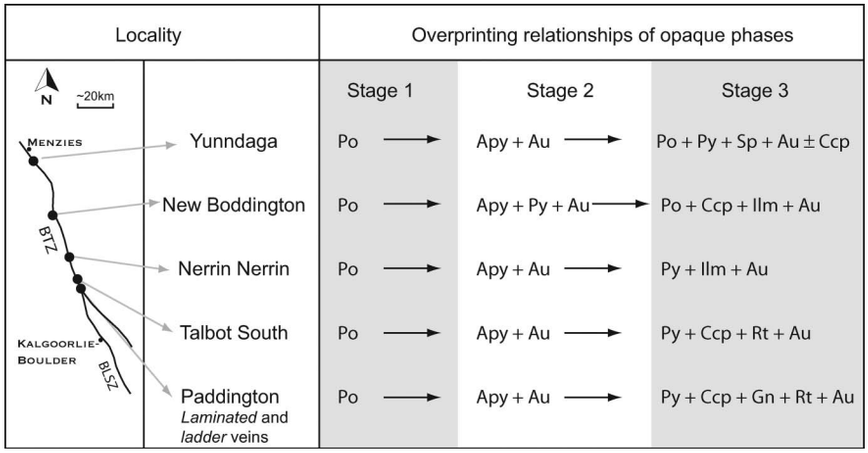

Figure 4 Schematic representation of the paragenesis of sulfide, oxide and visible gold phases from all studied localities. Apy, arsenopyrite; Au, visible/invisible gold; Ccp, chalcopyrite; Gn, galena; Ilm, ilmenite; Py, pyrite; Po, pyrrhotite; Rt, rutile; Sp, sphalerite.

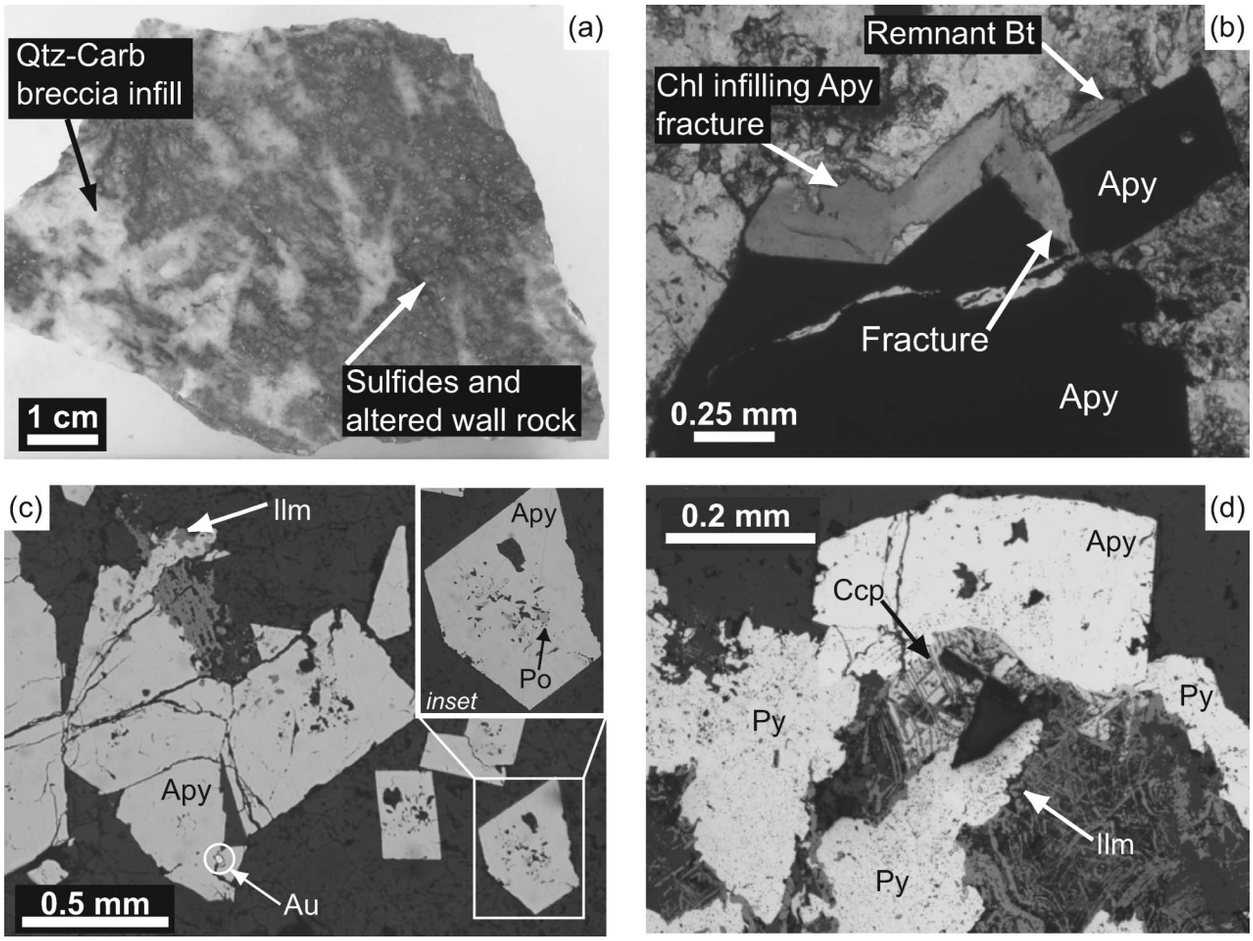

Figure 5 Photographs from the Talbot South gold deposit. (a) Brecciated ore. Note the abundance of sulfides in the altered wall-rock fragments (sample 10380 6C). (b) Photomicrograph of chlorite at the margin of a fractured arsenopyrite grain. Note remnant biotite in chlorite. Plane-polarised light, thin-section ~100 mm thick (sample BA02e). (c) Reflected-light photomicrograph of fractured arsenopyrite grains with visible gold in one fracture. Ilmenite has overprinted the arsenopyrite. Inset: close-up of an arsenopyrite grain with rounded remnant pyrrhotite inclusions (Stage 1) in its pitted core. Plane-polarised light (sample BA02b). (d) Reflected-light photomicrograph of a hydrothermally corroded arsenopyrite grain replaced by coliform pyrite and chalcopyrite, which is in turn overprinted by lenticular ilmenite grains. Plane-polarised light (sample BW-01). Bt, biotite; Apy, arsenopyrite; Au, visible gold; Ccp, chalcopyrite; Ilm, ilmenite; Py, pyrite. All samples reposited at School of Geosciences, Monash University.

wide wall-rock alteration assemblage dominated by carbonate (ferroan calcite), quartz, chlorite and muscovite (Table 1) and including arsenopyrite, pyrite, ilmenite, pyrrhotite and visible gold. From EDS analyses, the carbonate grains are characterised by a Ca-rich chemistry, generally with <5 atomic % Fe.

Analogous to the characteristics of alteration minerals already described at Paddington and Talbot South, Stage 1 remnant pyrrhotite inclusions occur in Stage 2 arsenopyrite. Stage 2 arsenopyrite grains were later fractured and overprinted by Stage 3 pyrite, visible gold and ilmenite (Figures 4, 6b, c). In addition to the alteration mineral paragenesis reported here, Manly (2003) noted the geometry of gold-bearing veins at Nerrin Nerrin to be similar to those at Paddington.

New Boddington deposit

The New Boddington gold deposit (<1 t produced Au) is situated approximately halfway between Paddington and Menzies (Figure 1). The north-northwest-trending host-rocks exposed in the openpit include a talc–chlorite schist (i.e. ultramafic unit) on its western margin, and a basaltic rock unit in the central and eastern parts of the pit (Figure 2c). There are also two interflow carbonaceous shale units (both <1 m thick) in the mafic sequence (Colville *et al.* 1990). All contacts are sheared and dip steeply to the west. Gold-bearing veins are hosted in the basalt unit and occur as stockwork and planar veins (Colville *et al.* 1990).

Access restrictions prohibited the recovery of *in situ* stockwork ore samples, and hence displaced blocks of foliated ore-bearing basalt sourced from the openpit ramp were used to characterise hydrothermal alteration and gold mineralisation (Figure 7a). The alteration assemblage proximal to the stockwork vein consists of carbonate (ferroan calcite), quartz, biotite (partly altered to chlorite), muscovite, sulf-arsenides, sulfides and ilmenite (Figure 7b). Biotite is more abundant here than at Paddington, Talbot South or Nerrin Nerrin, but the sulfur-bearing minerals are still dominated by arsenopyrite, with lesser pyrite, pyrrhotite and chalcopyrite.

As with the sulfur-bearing and oxide assemblages from Paddington, Talbot South and Nerrin Nerrin, arsenopyrite-dominated ore samples from New Boddington preserve Stage 1 pyrrhotite inclusions in Stage 2 arsenopyrite grains (Figure 4). Fractured arsenopyrite grains are zoned, with relatively pitted cores, and bordered by muscovite-bearing strain shadows, which are parallel to the pervasive foliation (Figure 7b). Stage 3 pyrrhotite, chalcopyrite and ilmenite overprint arsenopyrite, and fractures in arsenopyrite are partly filled with Stage 3 visible gold (Figure 7c). Unlike Paddington, Talbot South and Nerrin Nerrin, the ore paragenesis at New Boddington lacks Stage 3 pyrite, and pyrrhotite is also present during this alteration stage (Figure 4).

Yunndaga deposit

The Yunndaga gold deposit is located 6 km south of the township of Menzies and is the largest known gold deposit at the northern end of the Bardoc Tectonic Zone, having yielded 11 t of gold from historical (1895–1943) and recent (1995–1998) mining activities (Evans 2003). All rock units in the openpit trend towards the northwest and dip moderately to steeply towards the west. Exposed rock units on the western side of the pit mainly comprise a folded and foliated sequence of interlayered micaceous sandstones and shales, with a less extensive ultramafic layer, and a carbonaceous shale unit up to 5 m thick. A dolerite unit is exposed in the centre of the openpit and is flanked on its eastern side by micaceous sandstones and lesser interbedded shales (Figure 2d) (Beeson *et al.* 1996; this study). Beeson *et al.* (1996) and Witt (1993) reported lower amphibolite facies peak metamorphic conditions in the northern Bardoc Tectonic Zone.

Gold mineralisation is associated with a layer-parallel, laminated to massive quartz–carbonate shear vein, hosted in the dolerite near its western contact with the carbonaceous shale (Figures 2d, 8a). Witt (1992, 1993) also reported that a now inaccessible ultramafic unit also hosted gold mineralisation. The mafic wall-rock alteration assemblage directly adjacent to this vein consists of quartz, carbonate (ferroan calcite and siderite), biotite, muscovite, sulf-arsenides, sulfides, minor chlorite and epidote. In decreasing order of abundance, the sulfur-bearing minerals comprise arsenopyrite, pyrrhotite, sphalerite and chalcopyrite, together with visible gold. Chlorite primarily occurs in arsenopyrite fractures. The exact metamorphic conditions during the mineralising event(s) cannot be determined without a detailed study of the hydrothermal phases. However, the presence of biotite and epidote in textural equilibrium with the mineralised assemblages provides evidence that metamorphic conditions during mineralisation probably reached lower amphibolite facies. Lower amphibolite metamorphic conditions are further supported by hornblende and biotite assemblages preserved in the dolerite unit 10 m from the mineralised laminated vein. Metamorphic hornblende is not observed in gold deposits of the southern Bardoc Tectonic Zone, where greenschist-facies assemblages are stable (Witt 1993; Beeson *et al.* 1996; Mikucki & Roberts 2004). Despite these differences, the overprinting relationships of gold-bearing sulf-arsenide, sulfide and oxide phases are still similar to the other localities investigated. Stage 2 arsenopyrite grains also contain abundant Stage 1 pyrrhotite inclusions (Figure 8c). Furthermore, Stage 2 arsenopyrite grains are fractured and infilled with Stage 3 pyrite, pyrrhotite, sphalerite, minor chalcopyrite and visible gold (Figures 4, 8c, d). Similar to New Boddington, pyrrhotite is associated with Stage 3 alteration (Figure 8e), but unlike all other deposits there are no Ti-bearing oxides observed in the mineralised assemblage.

GOLD IN SULFIDES FROM THE BARDOC TECTONIC ZONE

Optical and SEM backscatter images show that visible gold is found in arsenopyrite fractures and along its margins, related to Stage 3 hydrothermal alteration (Figure 4). However, gold in orogenic systems also occurs commonly as sub-microscopic or invisible grains in sulfides (Cathelineau *et al.* 1989). Only particulate (free milling) gold was recovered from the Paddington deposit (Booth 1989), although quantitative LA-ICP-MS analysis reveals that Stage 2 arsenopyrite grains from all five localities contain gold in trace amounts of up to 28 ppm. Silver in these samples remains below detection

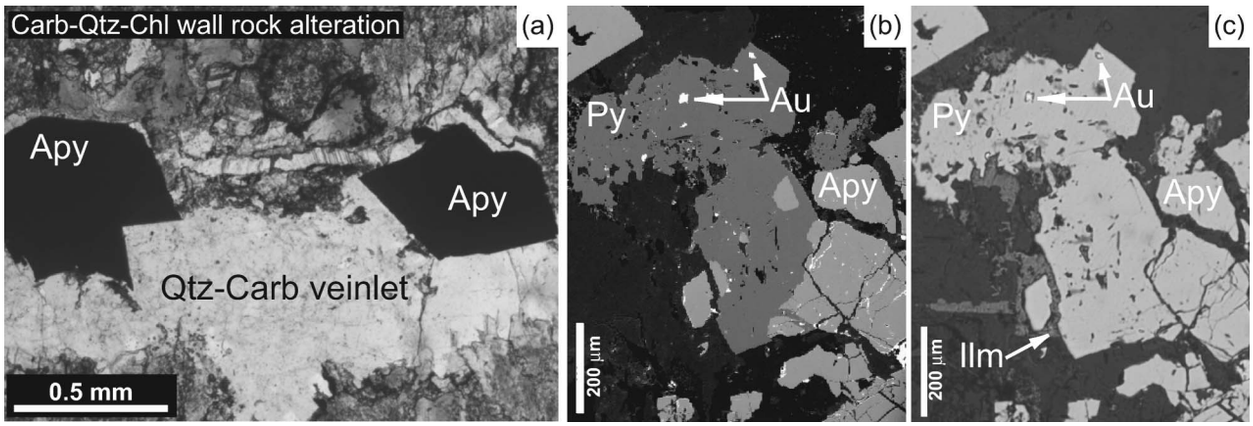

Figure 6 Photographs of rock samples collected from the Nerrin Nerrin exploration drillhole. (a) Transmitted-light photomicrograph of hydrothermal sulfide (opaque), carbonate, chlorite wall-rock proximal to quartz–carbonate veinlets. Plane-polarised light (sample NNDD0001C-Nc). (b) Backscatter SEM image of Stage 3 visible gold inclusions and pyrite that both infill fractures in Stage 2 arsenopyrite (sample NNDD001B-Nc). (c) Photomicrograph of (b), showing Stage 3 ilmenite overgrowing and infilling a fractured arsenopyrite fragment. Note that in reflected light it is difficult to discriminate between Stage 2 arsenopyrite and Stage 3 pyrite. Apy, arsenopyrite; Au, visible gold; Carb, carbonate; Chl, chlorite; Ilm, ilmenite; Py, pyrite; Qtz, quartz. All samples reposited at School of Geosciences, Monash University.

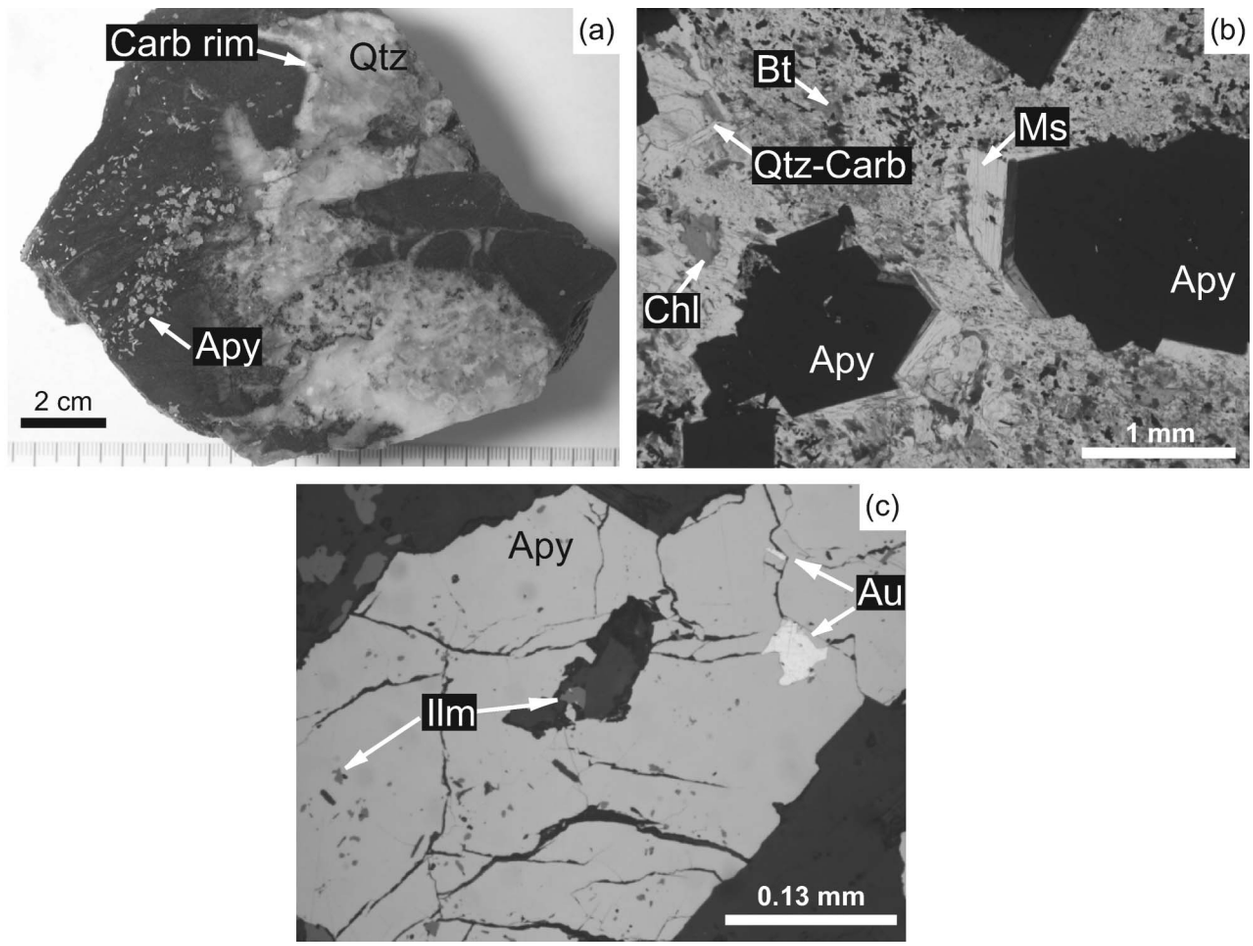

Figure 7 Photographs from the New Boddington gold deposit. (a) Deformed stockwork ore, with its associated carbonate, quartz, biotite, muscovite, chlorite and sulfide alteration assemblage (sample BWRCD326B). (b) Photomicrograph in transmitted light showing characteristic hydrothermal alteration, with biotite, chlorite and muscovite in arsenopyrite (opaque) strain shadows. Plane-polarised light (sample GG011906B7). (c) Photomicrograph in reflected light showing a Stage 2 arsenopyrite grain where fractures are infilled with Stage 3 visible gold + ilmenite (sample GG011906B5). Apy, arsenopyrite; Au, visible gold; Carb, carbonate; Chl, chlorite; Ilm, ilmenite; Py, pyrite; Qtz, quartz. All samples reposited at School of Geosciences, Monash University.

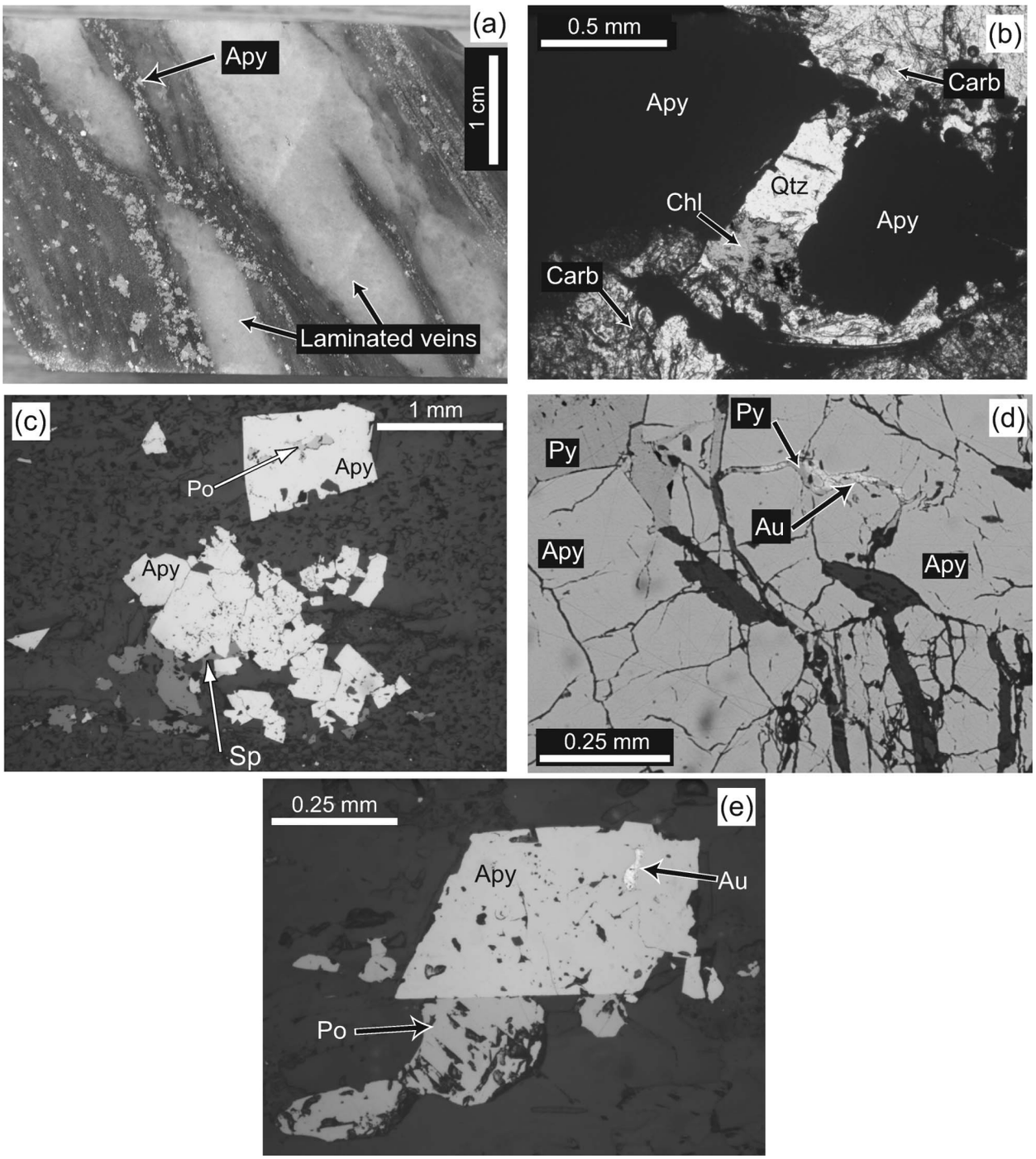

Figure 8 Photographs from the Yunndaga gold deposit. (a) The mineralised and boudinaged laminated vein from Yunndaga, showing arsenopyrite, carbonate, quartz, biotite, chlorite wall-rock alteration assemblage (sample YD10800). (b) Photomicrograph of an arsenopyrite grain (opaque) in a quartz, carbonate, biotite and chlorite alteration assemblage. Cross-polarised light (sample YU0FBcarb04). (c) Reflected-light photomicrograph showing Stage 1 pyrrhotite inclusions in Stage 2 arsenopyrite and Stage 3 sphalerite. Plane-polarised light (sample YD108004). (d) Reflected-light photomicrograph of fractured Stage 2 arsenopyrite grains infilled with Stage 3 pyrite and visible gold. Plane-polarised light (sample YDL1). (e) Reflected-light photomicrograph showing a Stage 3 visible gold particle in a Stage 2 arsenopyrite grain that is rimmed by Stage 3 pyrrhotite. Plane-polarised light (sample YD108003). Apy, arsenopyrite; Carb, carbonate; Po, pyrrhotite; Py, pyrite; Qtz, quartz; Sp, sphalerite. All samples reposited at School of Geosciences, Monash University.

limits (Table 4; Figure 9). Analyses failed to detect elevated concentrations of sub-microscopic gold in Stage 3 pyrite. In all cases, SEM backscattered images were used to ensure ablation spots were away from any fractures in Stage 2 arsenopyrite and other visible gold grains. As typified in Figure 9, the gold signal in arsenopyrite is relatively uniform with no noticeable spikes in the ablation analyses, which are used here to

suggest that gold is sub-microscopic and uniformly dispersed throughout arsenopyrite. From this, we conclude that sub-microscopic or invisible gold is associated with Stage 2 arsenopyrite, whereas visible gold is associated with the Stage 3 influx of pyrite, base-metal sulfides and Fe oxides.

A structural and alteration study of the Aphrodite prospect (Crameri 2002), situated between Nerrin Nerrin and New Boddington (Figure 1), reported that gold in pyrite–arsenopyrite ore assemblages was refractory. No details were provided regarding the relative overprinting relationships of the sulfide phases and therefore more research needs to be conducted at Aphrodite to establish the paragenesis of gold at this prospect and relevance to other deposits in the Bardoc Tectonic Zone.

SULFUR ISOTOPE DATA

Fifty-six *in situ* and four conventional sulfur isotope analyses were conducted on samples from the Bardoc Tectonic Zone (Tables 2, 3), including 41 analyses on Stages 2 and 3 arsenopyrite and pyrite (Figure 10a), and 18 analyses on unmineralised, pyrite-bearing carbonaceous shale units that outcrop in all openpits studied (Figures 2a–d, 10b). One mineralised gabbro (whole-rock sample) from Talbot South was also analysed to compare with *in situ* analyses on the sulfides and sulf-arsenides.

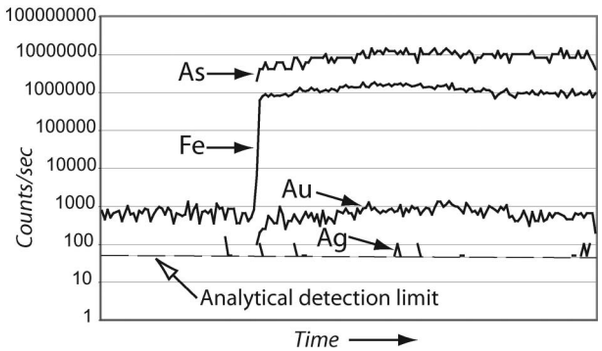

Figure 9 Representative LA-ICP-MS analysis graph used to calculate the concentration of invisible gold in Stage 2 arsenopyrite. Arsenic, iron, gold and silver traces shown only. The detection limit for the analysis run is also indicated (dashed line). Note that the gold trace is uniform without spikes, suggestive of a uniform distribution of gold within the ablated arsenopyrite grain. Data from the ladder vein (Table 4), Paddington gold deposit.

In situ and conventional δ^{34} sulfur isotope analyses on Stage 2 arsenopyrite and Stage 3 pyrite from all localities yielded values ranging from 0 to +9‰ (Figure 10a), with no distinct clustering of data from deposit to deposit (Tables 2, 3; Figure 10a). The average δ^{34}S value of Stage 2 arsenopyrite grains is $+5.8 \pm 0.6$‰, and varies between +1 and +9‰. In contrast, the average δ^{34}S composition of Stage 3 pyrite grains is $+3.6 \pm 0.6$‰, with a range from 0 to +7‰. This difference, albeit relatively minor, can be accounted for by numerous competing factors, including different sulfur isotope fractionation factors for arsenopyrite and pyrite, the state of equilibrium between the sulfur species and the sulfides during each stage, oxygen fugacity or redox state of the hydrothermal system and the source of sulfur in the different phases (Ohmoto & Goldhaber 1997). In spite of this, the range of δ^{34} sulfur values of sulfides from Bardoc Tectonic Zone samples is relatively narrow, as opposed to the broad range of δ^{34} sulfur compositions from world-class gold deposits elsewhere in the Eastern Goldfields Province (Phillips *et al.* 1986; Weinberg *et al.* 2002). Stage 3 pyrrhotite, which has only been observed at New Boddington and Yunndaga, yields δ^{34}S values of +3.5 and $+0.1 \pm 0.4$‰, respectively (Figure 10a). The presence of pyrrhotite requires reduced hydrothermal conditions, and under these conditions the fractionation of δ^{34}S into pyrrhotite from an H_2S– fluid is negligible (Ohmoto & Goldhaber 1997), so that the above δ^{34}S values can be considered as representative of a reduced fluid source. Stage 1 pyrrhotite inclusions were not analysed, as they were too small for *in situ* analysis.

The sulfur isotope composition of pyrite in unmineralised sedimentary rocks, as determined from conventional and *in situ* analyses proximal to mineralised mafic rocks (Table 3; Figure 10b), yields an average δ^{34}

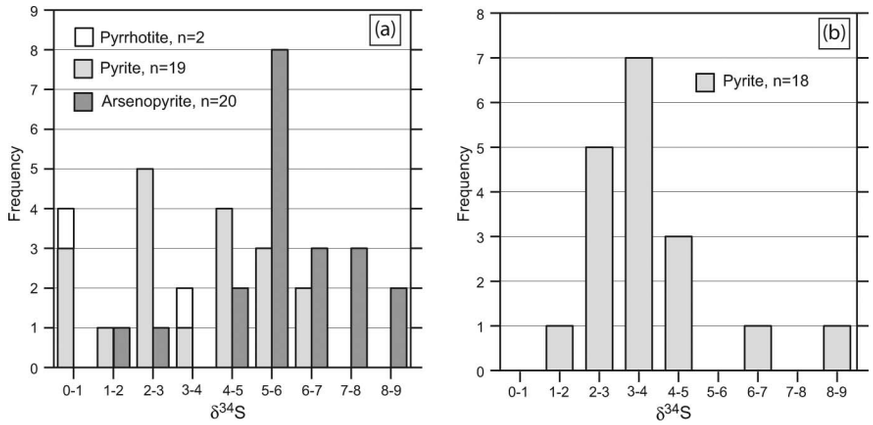

Figure 10 (a) Distribution of δ^{34}S (‰) values from gold-bearing arsenopyrite and pyrite from all study locations. Pyrrhotite analyses are only from New Boddington and Yunndaga. (b) Distribution of δ^{34}S (‰) values from unmineralised pyritic sedimentary units adjacent to the mineralised mafic rocks. See Tables 2 and 3 for related data.

sulfur value of $+3.9 \pm 0.6$‰, and ranges between +1.4 and +8.0‰, which is broadly identical to those in mineralised samples. Conventional analysis of a mineralised whole-rock sample from Talbot South yielded $+2.25 \pm 0.15$‰ (Table 2), well within the δ^{34} sulfur range of the sulfide separates, and further suggests that there were no highly positive or negative sulfur isotope species associated with the mineralised assemblage.

DISCUSSION

Orogenic-gold deposits in the Eastern Goldfields Province have a considerable variety of host-rocks, structural, mineralogical and alteration characteristics (Hagemann & Cassidy 2001; Witt & Vanderhor 1998). This contrasts with the wide and anastomosing shear system that defines the Bardoc Tectonic Zone, where gold deposits have a number of uniform features, such as (Table 5): (i) similar opaque mineral assemblages dominated by arsenopyrite; (ii) a similar hydrothermal evolution characterised by three distinct stages (Figure 4) taking place over one broad deformation event (Morey *et al.* 2005); (iii) narrow arsenopyrite and pyrite δ^{34}S values, ranging between 0 and +9‰, suggestive of a reducing hydrothermal environment; and (iv) a lack of hydrothermal minerals that are associated with oxidising conditions (i.e. hematite and sulfates). These features do not vary despite differences in the style of the quartz–carbonate veins (Table 1), and the range of metamorphic grades of the host mafic units (greenschist facies in the southern Bardoc Tectonic Zone and lower amphibolite facies metamorphism in the Yunndaga region: Witt 1992, 1993).

Many of these similarities in mineralisation could be due to the similar host-rocks of the deposits studied (i.e. mafic units). However, hydrothermal alteration and mineralogical characteristics of gold deposits hosted by mafic rocks in the Boulder–Lefroy Shear Zone (e.g. Golden Mile, Mt. Charlotte and St. Ives) (Table 5) and elsewhere in the Eastern Goldfields Province (Ora Banda Domain and Norseman gold camp: Harrison *et al.* 1990; McCuaig *et al.* 1993) are significantly different to those in the Bardoc Tectonic Zone (Table 5). Furthermore, commonality in host-rocks alone cannot explain the more profound similarities implied by the uniform three-stage evolution of the opaque minerals documented over a strike length of 80 km. This requires that the evolutionary path of the mineralising fluids from source to deposit, and interaction with host rock, be similar. The profound similarities among these mafic-hosted gold deposits allow the definition of Bardoc-style mineralisation, which is characteristic of the small- to moderate-size (<40 t gold), mafic-hosted deposits within this broad anastomosing shear system. Other rock units in the Bardoc Tectonic Zone also host gold mineralisation, including ultramafic and sedimentary rocks (Witt 1993), and these deposits may have different alteration characteristics. However, the hydrothermal conditions during gold mineralisation suggested from this regional study (i.e. uniformly reduced pyrrhotite–arsenopyrite–pyrite environments) are also considered to be applicable to other lithologies.

Past studies (Weinberg *et al.* 2004; Hodkiewicz *et al.* 2005) have linked the Paddington deposit with the Boulder–Lefroy Shear Zone system: however, our study demonstrates that the style, stages of alteration and setting of gold mineralisation at the Paddington deposit are similar to those of the other Bardoc Tectonic Zone localities (Figure 4). This is consistent with the view that, despite generally being considered to be part of the Boulder–Lefroy Shear Zone, Paddington is more likely part of the Bardoc Tectonic Zone lying at a complex intersection between a number of shear systems, close to the boundary between the Boulder–Lefroy Shear Zone and the Bardoc Tectonic Zone.

We speculate that the small to moderate size of the Bardoc Tectonic Zone gold deposits is a key feature of this style, and results from the relatively planar and highly strained nature of the Bardoc Tectonic Zone, and the nature of the mineralising fluids that permeated the system. Since the Boulder–Lefroy Shear Zone is connected to the Bardoc Tectonic Zone, a comparison between the deposits of these two adjoining shear systems may highlight features that discriminate large and small orogenic-gold deposits in the Eastern Goldfields Province (Table 5). Distinguishing features between these two shear systems are: (i) the Boulder–Lefroy Shear Zone is a narrow, variably striking shear zone, compared with a more constant strike and widespread shearing in the Bardoc Tectonic Zone (Hodkiewicz *et al.* 2005); (ii) gold deposits associated with the Boulder–Lefroy Shear Zone record a greater variety of deformation and gold mineralisation events (Bateman & Hagemann 2004; Weinberg *et al.* 2005); (iii) the Boulder–Lefroy Shear Zone has a greater abundance of sedimentary rock units bounding the shear system and thicker mafic units hosting gold mineralisation; and (iv) gold deposits/camps associated with the Boulder–Lefroy Shear Zone are located proximal to regional antiformal structures, such as the Boomerang Anticline and the New Celebration Anticline (Figure 1). Thus, the two connected shear systems display a number different geological features that may have played an important role in controlling the nature of hydrothermal alteration and gold mineralisation within each respective shear system.

The range of δ^{34}S compositions of gold-bearing sulfides from this study (0 to +9‰: Figure 10) is similar to those typical of Archaean orogenic-gold deposits in the Eastern Goldfields Province and elsewhere (Lambert *et al.* 1984; McCuaig & Kerrich 1998), and indicate that overall reduced hydrothermal conditions prevailed during gold mineralisation in the Bardoc Tectonic Zone. These uniform S-isotope data further support mineral and paragenetic relationships from the Bardoc Tectonic Zone (Figure 4) that indicated the ore fluid related to gold mineralisation was similar throughout the whole shear system (Salier *et al.* 2005). However, some world-class mafic-hosted deposits associated with the Kalgoorlie and Kambalda gold camps along the Boulder–Lefroy Shear Zone (Figure 1) (Phillips *et al.* 1986; Weinberg *et al.* 2002; Neumayr *et al.* 2004), as well as some other world-class deposits in the Eastern Goldfields Province (e.g. Sunrise Dam, Tarmoola and Kanowna Belle: Ren *et al.* 1994; Weinberg *et al.* 2002; Brown *et al.* 2003) have a

Table 5 Comparison between gold deposits of the Bardoc Tectonic Zone and the Boulder–Lefroy Shear Zone.

	Bardoc Tectonic Zone	Boulder-Lefroy Shear Zone	Source
Past production (t Au)	~100	>2000	Witt (1992, 1993)
Major host units for gold mineralisation	Mafic extrusive and intrusive rocks	Mafic extrusive and intrusive rocks	Witt (1993)
Thickness of individual host units	<100 m	<700 m	Witt (1993); Phillips *et al.* (1996)
Width of shear system	<12 km	<2 km	Witt (1993) Cox and Ruming (2004)
Gold deposits located within subordinate shear system(s)?	No, located within broad deformation zone	Yes, except for New Celebration	Weinberg *et al.* (2005)
Association with regional antiformal structures	Only synformal closures preserved, not associated with gold	Boomerang antiform Celebration antiform St. Ives antiform	Swager and Griffin (1990b); Beeson *et al.* (1996)
Strike of shear system in plan view	Relatively linear, less than 10° variation	Variable strike, more than 10° variation	Weinberg *et al.* (2004); Hodkiewicz *et al.* (2005)
N–S deformation and thrust stacking (D_1)	Not documented	Well developed within the southern part of zone	Swager and Griffin (1990b); Morey *et al.* (2005)
Major ENE–WSW shortening (D_2)	Well developed	Well developed	Morey *et al.* (2005); Weinberg *et al.* (2005)
Strike-slip deformation (D_3)	D_2 sinistral component only at Menzies	Well-developed D_3 sinistral	Morey *et al.* (2005); Weinberg *et al.* (2005)
Strike-slip brittle deformation (D_4)	Well developed	Well developed	Morey *et al.* (2005) Weinberg *et al.* (2005)
Relative timing of gold mineralisation	Associated with D_2	Associated with D_2, D_3 and D_4	Morey *et al.* (2005) Weinberg *et al.* (2005)
Major silicate and carbonate alteration minerals[a]	Cal, Qtz, Mus, Chl ± Bt ± Sd	Qtz, Ank, Ser, Ms, Anh (rare), Ab	Hagemann and Cassidy (2001); This study
Sulfide, sulfate and oxide alteration minerals[a]	Apy, Py, base-metal sulfides, Po, Ilm, Rt	Py, Hem (rare), Mag, Apy, Rt, Po, sulfates	Hagemann and Cassidy (2001); this study
Sulfur isotopes $\delta^{34}S$ (‰)	0 to +9	−10 to +10	Phillips *et al.* (1986); Weinberg *et al.* (2002); this study

[a]Ab, albite; Anh, anhydrite; Ank, ankerite; Apy, arsenopyrite; Bt, biotite; Cal, calcite; Chl, chlorite; Hem, hematite; Ilm, ilmenite; Mag, magnetite; Ms, muscovite; Po, pyrrhotite; Py, pyrite; Qtz, quartz; Rt, rutile; Sd, siderite; Ser, sericite.

broader range, with a combined distribution of $\delta^{34}S_{pyrite}$ from −10‰ to +10‰. Salier *et al.* (2005) accounted for the more negative $\delta^{34}S_{pyrite}$ and $\delta^{34}S_{galena}$ values (between −5.7‰ and +0.9‰) at the Jupiter deposit, Laverton, through reduced fluids reacting with a pre-existing, more oxidised host unit that fractionated the sulfur in sulfides to a greater degree. However, the larger sulfur isotopic variations associated with many world-class gold deposits in the Eastern Goldfields Province (summarised in Weinberg *et al.* 2002) are possibly due to more oxidised environments during gold mineralisation (Lambert *et al.* 1984; Phillips *et al.* 1986; Cameron & Hattori 1987). For the smaller Bardoc Tectonic Zone deposits, minerals indicative of reduced hydrothermal conditions (i.e. pyrrhotite and ilmenite) are consistently documented either as Stage 1 or as Stage 3 minerals (Figure 4), and as such, may potentially be used to discriminate between large (>100 t Au) and smaller gold deposits in orogenic-gold provinces.

The observed shift from pyrrhotite (Stage 1) to pyrite and rutile (Stage 3) in the Bardoc Tectonic Zone deposits (Figure 4) can be explained through a relatively minor increase in fluid oxygen fugacity. Although possible, this proposed oxidation is likely to be minimal or insignificant, as no noteworthy change of the isotopic values from Stage 1 pyrrhotite to Stage 3 pyrite could be observed (Figure 10). Other studies have also argued that significant variations in redox could be due to the influence of mineralising fluids from granites (Mueller *et al.* 1991) or fluid mixing (Neumayr *et al.* 2003; Walshe *et al.* 2003), with the latter studies speculating that these processes were a prerequisite to form large (>100 t Au) gold deposits. The lack of more significant variations in $\delta^{34}S$ values of sulfides from the Bardoc Tectonic Zone deposits (Figure 10) does not support redox changes or fluid mixing as the main gold mineralisation mechanism(s), and reflects more uniform hydrothermal conditions, linked here with the formation of relatively small (<100 t Au) gold deposits.

Pyrite grains in the unmineralised carbonaceous shale units that straddle mineralised lithologies (Figure 2) have similar $\delta^{34}S$ values and ranges to mineralised pyrite (Figure 10). Other unmineralised, sedimentary-hosted pyrite grains from the Eastern Goldfields Province similarly range between 0‰ and 12‰, with an average of 5.5‰ (Weinberg *et al.* 2002). If the sedimentary-hosted sulfur is considered diagenetic, the sedimentary units could have acted as a source of sulfur for the mineralised arsenopyrite and pyrite in the proximal mafic units. However, due to the unmineralised pyrite grains being significantly affected by deformation and silica infiltration, it is also possible that both types of sulfides have a hydrothermal origin, or the available stable isotopic data are insufficient to discriminate between each pyrite (unmineralised *vs* mineralised) phase.

CONCLUSIONS

The Bardoc Tectonic Zone is an intensely deformed, broad deformation zone (<12 km wide in plan view), in which only small- to moderate-sized gold deposits (<40 t produced gold) have been discovered to date. Results herein illustrate that the mineralisation style along the length of this shear system is very similar, allowing for the definition of 'Bardoc-style' gold mineralisation. This style is typified by a three-stage wall-rock alteration history within competent, mafic host rocks (Figure 4), developed during a major deformation event under reduced hydrothermal conditions. Sulfur-bearing minerals associated with wall-rock alteration haloes are dominated by arsenopyrite, with reducing mineral assemblages and a restricted range of sulfur isotope values (Figure 10; Tables 2, 3). This mineralisation style is also typified by the absence of phases indicative of oxidised hydrothermal conditions and the absence of tellurides, and gold deposits are hosted directly within a wide (between 5 and 12 km across strike) shear zone (Figure 1). These shared features differ significantly from many giant and world-class gold deposits in the Eastern Goldfields Province in general and the Boulder–Lefroy Shear Zone in particular, and are inferred here to be the reason why the known gold deposits in the Bardoc Tectonic Zone are considerably lesser endowed. Bardoc-style deposits show little sensitivity to changes in vein style and the metamorphic grade of the host mafic unit (between greenschist and lower amphibolite facies). The definition of a geographically constrained style of mineralisation allows for more specific exploration targeting in this corridor of deformed supracrustal rocks.

ACKNOWLEDGEMENTS

Results reported herein form part of AAM's PhD work and have been released with permission from the CEO, *predictive mineral discovery** Cooperative Research Centre. Stafford McKnight (SEM, EDS), Keith Harris and Christine Cook (stable isotope analyses), Sarah Gilbert and Leonid Danyushevsky (LA-ICP-MS analyses) and Robert Douglas and Simon Stephens (rock sample preparation) are thanked for their invaluable assistance. Placer Dome Asia Pacific (now Barrick Gold Corporation) is gratefully acknowledged for supporting fieldwork and allowing drill core access. David Groves and Andy Wilde are thanked for their critical feedback on draft versions of this study, and Brett Davis and Bruce Groenewald for their formal reviews. AAM thanks the Society of Economic Geologists for a Newmont Student Research Grant Award, which helped facilitate stable sulfur isotope analyses.

REFERENCES

ALARDYCE W. & VANDERHOR F. 1998. Paddington. *In*: Vanderhor F. & Groves D. I. eds. *Systematic Documentation of Archaean Gold Deposits of the Yilgarn Block*, pp. 115–119. MERIWA Report **193(II)**.

BATEMAN R. & HAGEMANN S. G. 2004. Gold mineralisation throughout about 45 Ma of Archaean orogenesis: protracted flux of gold in the Golden Mile, Yilgarn Craton, Western Australia. *Mineralium Deposita* **39**, 536–559.

BEESON J., DE LUCA K., FLANAGAN D., GYNGELL N. & SMITHSON A. 1996. Geology of the Bardoc Tectonic Zone, Western Australia. Goldfields Exploration Pty Ltd internal report (unpubl.).

BOOTH W. 1989. The mineralogy, geology and exploration geochemistry of the Paddington Gold Mine, Broad Arrow, Western Australia. PhD thesis, University of New South Wales, Sydney (unpubl.).

BROWN S. M., JOHNSON C. A., WATLING R. J. & PREMO W. R. 2003. Constraints on the composition of ore fluids and implications for mineralising events at the Cleo gold deposit, Eastern Goldfields Province, Western Australia. *Australian Journal of Earth Sciences* **50**, 19–38.

CAMERON E. M. & HATTORI K. 1987. Archean gold mineralization and oxidized hydrothermal fluids. *Economic Geology* **82**, 1177–1191.

CATHELINEAU M., BOIRON M. C., HOLLIGER P., MARION P. & DENIS M. 1989. Gold in arsenopyrites; crystal chemistry, location and state, physical and chemical conditions of deposition. *In*: Keays R. R., Ramsay W. R. H. & Groves D. I. eds. *The Geology of Gold Deposits; the Perspective In 1988*, pp. 328–341. Economic Geology Monograph **6**.

COLVILLE R. G., KELLY D. & FISH B. L. 1990. Goongarrie gold deposits. *In*: Hughes F. E. ed. *Geology of the Mineral Deposits of Australia and Papua New Guinea*, pp. 363–366. Australasian Institute of Mining and Metallurgy Monograph **14**.

COX S. F. & RUMING K. 2004. The St Ives mesothermal gold system, Western Australia—a case of golden aftershocks? *Journal of Structural Geology* **26**, 1109–1125.

CRAMERI K. 2002. Structural controls on mineralisation within the Alpha Lode at the Aphrodite deposit, Western Australia, BSc (Hons) thesis, University of South Australia, Adelaide (unpubl.).

DANYUSHEVSKY L., ROBINSON P., MCGOLDRICK P., LARGE R. R. & GILBERT S. 2003. Quantitative multi-element analysis of sulphide minerals by laser ablation ICPMS. *Geological Society of Australia Abstracts* **73**, 260.

DAVIS B. K. & MAIDENS E. 2003. Archaean orogen-parallel extension: evidence from the northern Eastern Goldfields Province, Yilgarn Craton. *Precambrian Research* **127**, 229–248.

EISENLOHR B. N., GROVES D. & PARTINGTON G. A. 1989. Crustal-scale shear zones and their significance to Archaean gold mineralization in Western Australia. *Mineralium Deposita* **24**, 1–8.

EVANS W. 2003. Yunndaga Review. Placer Dome Asia Pacific Internal Memorandum (unpubl.).

GOLEBY B. R., KORSCH R. J., FOMIN T., BELL B., NICOLL M. G., DRUMMOND B. J. & OWEN A. J. 2002. Preliminary 3-D geological model of the Kalgoorlie region, Yilgarn Craton, Western Australia, based on deep seismic-reflection and potential-field data. *Australian Journal of Earth Sciences* **49**, 917–933.

GROVES D. I. 1993. The crustal continuum model for late-Archaean lode-gold deposits of the Yilgarn Block, Western Australia. *Mineralium Deposita* **28**, 366–374.

GROVES D. I., GOLDFARB R. J., GEBRE-MARIAM M., HAGEMANN S. G. & ROBERT F. 1998. Orogenic gold deposits; a proposed classification in the context of their crustal distribution and relationship to other gold deposit types. *Ore Geology Reviews* **13**, 7–27.

GROVES D. I., PHILLIPS G. N., HO S. E., HENDERSON C. A., CLARK M. E. & WOAD G. M. 1984. Controls on the distribution of Archaean hydrothermal gold deposits in Western Australia. *In*: Foster R. P. ed. *Gold '82: the Geology, Geochemistry and Genesis of Gold Deposits*, pp. 689–712. A. A. Balkema, Rotterdam.

HAGEMANN S. G. & CASSIDY K. F. 2001. World-class gold camps and deposits in the Eastern Goldfields Province, Yilgarn Craton: diversity in host rocks, structural controls, and mineralization styles. *In*: Hagemann S. G., Neumayr P. & Witt W. K. eds. *World-class Gold Camps and Deposits in the Eastern Yilgarn Craton, Western Australia, with Special Emphasis on the Eastern Goldfields Province*, pp. 7–44. Geological Survey of Western Australia Record **2001/17**.

HANCOCK M. C., ROBERTSON I. G. & BOOTH G. W. 1990. Paddington gold deposits. *In*: Hughes F. E. ed. *Geology of the Mineral Deposits of Australia and Papua New Guinea*, pp. 395–400. Australasian Institute of Mining and Metallurgy Monograph **14**.

HARRISON N., BAILEY A., SHAW J. D., PETERSEN G. N. & ALLEN C. A. 1990. Ora Banda gold deposits. *In*: Hughes F. E. ed. *Geology of the Mineral Deposits of Australia and Papua New Guinea*, pp. 389–394. Australasian Institute of Mining and Metallurgy Monograph **14**.

HODKIEWICZ P. F., WEINBERG R. F., GARDOLL S. J. & GROVES D. 2005. Complexity gradients in the Yilgarn Craton: fundamental controls on crustal-scale fluid flow and the formation of world-class orogenic-gold deposits. *Australian Journal of Earth Sciences* **52**, 831–841.

HUNTER W. M. 1993. Geology of the granite–greenstone terrane of the Kalgoorlie and Yilma 1:100 000 sheets, Western Australia. *Geological Survey of Western Australia Report* **35**.

HUSTON D. L., POWER M., GEMMELL J. B. & LARGE R. R. 1995. Design, calibration and geological application of the first operational Australian laser ablation sulphur isotope microprobe. *Australian Journal of Earth Sciences* **42**, 549–555.

KRETZ R. 1983. Symbols for rock-forming minerals. *American Mineralogist* **68**, 277–279.

LAMBERT I. B., PHILLIPS G. N. & GROVES D. I. 1984. Sulphur isotope compositions and genesis of Archaean gold mineralization, Australia and Zimbabwe. *In*: Foster R. P. ed. *Gold '82: the Geology, Geochemistry and Genesis of Gold Deposits*, pp. 373–387. A. A. Balkema, Rotterdam.

MANLY M. A. 2003. Broad Arrow to Bardoc prospect and tenement review, Placer Dome Asia Pacific internal report (unpubl.).

MCCUAIG T. C. & KERRICH R. 1998. P–T–t deformation-fluid characteristics of lode gold deposits: evidence from alteration systematics. *Ore Geology Reviews* **12**, 381–454.

MCCUAIG T. C., KERRICH R., GROVES D. I. & ARCHER N. 1993. The nature and dimensions of regional and local gold-related hydrothermal alteration in tholeiitic metabasalts in the Norseman goldfields: the missing link in a crustal continuum of gold deposits? *Mineralium Deposita* **28**, 420–435.

MIKUCKI E. J. & ROBERTS F. I. 2004. Metamorphic petrography of the Kalgoorlie region, Eastern Goldfields granite–greenstone terrane: METPET database. *Geological Survey of Western Australia Record* **2003/12**.

MOREY A. A., WEINBERG R. F. & BIERLEIN F. P. 2005. Deformation history and multiple gold mineralisation events within the Bardoc Tectonic Zone, Eastern Goldfields, Western Australia. *In*: Mao J. & Bierlein F. P. eds. *8th Biennial SGA Meeting: Mineral Deposit Research: Meeting the Global Challenge*, pp. 557–560. Springer, Beijing.

MUELLER A. G., GROVES D. I. & DELOR C. P. 1991. The Savage lode magnesian skarn in the Marvel Loch gold–silver mine, Southern Cross greenstone belt, Western Australia: pressure–temperature and constraints on fluid sources. *Canadian Journal of Earth Sciences* **28**, 686–705.

NEUMAYR P., HAGEMANN S., HORN L., WALSHE J. L. & MORRISON R. 2004. Camp- to deposit-scale spatial zonation and temporal succession of redox indicator sulfide-oxide minerals: vectors to Archaean orogenic gold deposits; an example from the St. Ives gold camp, Yilgarn Craton, Western Australia. *Geological Society of Australia Abstracts* **73**, 105.

NEUMAYR P., HAGEMANN S. G., WALSHE J. L. & MORRISON R. S. 2003. Camp- to deposit-scale zonation of hydrothermal alteration in the St Ives gold camp, Yilgarn Craton, Western Australia: evidence for two fluid systems? *In*: Eliopoulos D. G. ed. *Mineral Exploration and Sustainable Development*, pp. 799–802. Millpress, Rotterdam.

NORMAN M., ROBINSON P. & CLARK D. 2003. Major- and trace-element analysis of sulfide ores by laser-ablation ICP-MS, solution ICP-MS, and XRF: new data on international reference materials. *The Canadian Mineralogist* **41**, 293–305.

OHMOTO H. & GOLDHABER M. B. 1997. Sulfur and carbon isotopes. *In*: Barnes H. L. ed. *Geochemistry of Hydrothermal Ore Deposits*, pp. 517–612. Wiley. New York.

PHILLIPS G. N., GROVES D. I. & KERRICH R. 1996. Factors in the formation of the giant Kalgoorlie gold deposit. *Ore Geology Reviews* **10**, 295–317.

PHILLIPS G. N., GROVES D. I., NEALL F. B., DONNELLY T. H. & LAMBERT I. B. 1986. Anomalous sulfur isotope compositions in the Golden Mile, Kalgoorlie. *Economic Geology* **81**, 2008–2015.

REN S. K., HEITHERSAY P. S. & BALINGER T. A. 1994. The Kanowna Belle gold deposit and implications to Archaean gold metallogeny of the Yilgarn Craton, Western Australia. *Proceedings of the 9th Quadrennial IAGOD Symposium, Beijing*, pp. 303–318.

REVELL N. 2000. Broad Arrow Pit Completion Report. Goldfields Limited (unpubl.).

ROBERT F. & BROWN A. C. 1986. Archean gold-bearing quartz veins at the Sigma Mine, Abitibi greenstone belt, Quebec. Part II, Vein paragenesis and hydrothermal alteration. *Economic Geology* **81**, 593–616.

ROBINSON B. W. & KASAKABE M. 1975. Quantitative preparation of sulphur dioxide for $^{34}S/^{32}S$ analyses from sulphides by combustion with cuprous oxide. *Analytical Chemistry* **47**, 1179–1181.

SALIER B. P., GROVES D. I., MCNAUGHTON N. J. & FLETCHER I. R. 2005. Geochronological and stable isotope evidence for widespread orogenic gold mineralization from a deep-seated fluid source at ca. 2.65 Ga in the Laverton Gold Province, Western Australia. *Economic Geology* **100**, 1363–1388.

SHEEHAN P. & HALLEY S. 2002. Paddington review. Paddington Gold Pty Ltd (unpubl.).

SWAGER C. P. 1997. Tectono-stratigraphy of late Archaean greenstone terranes in the southern Eastern Goldfields, Western Australia. *Precambrian Research* **83**, 11–42.

SWAGER C. P. & GRIFFIN T. J. 1990a. *Geology of the Archaean Kalgoorlie Terrane, Northern and Southern Sheets, 1:250 000.* Geological Survey of Western Australia, Perth.

SWAGER C. P. & GRIFFIN T. J. 1990b. An early thrust duplex in the Kalgoorlie–Kambalda greenstone belt. *Precambrian Research* **48**, 63–73.

SWAGER C. P., GRIFFIN T. J., WITT W. K., WYCHE S., AHMAT A. L., HUNTER W. M. & MCGOLDRICK P. J. 1995. Geology of the Archaean Kalgoorlie Terrane—an explanatory note. *Geological Survey of Western Australia Report* **48**.

WALSHE J. L., HALLEY S. W., HALL G. A. & KITTO P. 2003. Contrasting fluid systems, chemical gradients and controls on large-tonnage, high-grade Au deposits, Eastern Goldfields Province, Yilgarn Craton, Western Australia. *In*: Eliopoulos D. G. ed. *Mineral Exploration and Sustainable Development*, pp. 827–830. Millpress, Rotterdam.

WEINBERG R. F., GROVES D. I., HODKIEWICZ P. F. & VAN DER BORGH P. 2002. Hydrothermal systems, giant ore deposits and a new paradigm for predictive mineral exploration. *AMIRA Project P511, Yilgarn Atlas Vol. 3*, pp. 140–170 (unpubl.) <http://users.monash.edu.au/~weinberg/Yilgarn.htm>.

WEINBERG R. F., HODKIEWICZ P. F. & GROVES D. I. 2004. What controls gold distribution in Archean terranes? *Geology* **32**, 545–548.

WEINBERG R. F., MORESI L. & VAN DER BORGH P. 2003. Timing of deformation in the Norseman–Wiluna Belt, Yilgarn Craton, Western Australia. *Precambrian Research* **120**, 219–239.

WEINBERG R. F., VAN DER BORGH P., BATEMAN R. & GROVES D. I. 2005. Kinematic history of the Boulder–Lefroy Shear Zone System and controls on associated gold mineralization, Yilgarn Craton, Western Australia. *Economic Geology* **100**, 1407–1426.

WITT W. K. 1992. Gold deposits of the Menzies and Broad Arrow areas, Western Australia. Part 1 of a systematic study of the gold mines of the Menzies–Kambalda region. *Geological Survey of Western Australia Record* **1992/13**.

WITT W. K. 1993. Gold mineralisation of the Menzies–Kambalda Region, Eastern Goldfields, Western Australia. *Geological Survey of Western Australia Report* **39**.

WITT W. K. 1994. *Geology of the Bardoc 1:100 000 Sheet.* Geological Survey of Western Australia, Perth.

WITT W. K. & SWAGER C. P. 1989. Structural setting and geochemistry of Archaean I-type granites in the Bardoc–Coolgardie area of the Norseman–Wiluna Belt, Western Australia. *Precambrian Research* **44**, 323–351.

WITT W. K. & VANDERHOR F. 1998. Diversity within a unified model for Archaean gold mineralization in the Yilgarn Craton of Western Australia . . . an overview of the late-orogenic, structurally-controlled gold deposits. *Ore Geology Reviews* **13**, 29–64.

Received 13 June 2006; accepted 19 February 2007